ORIGINAL ARTICLE

Dispersion velocity revisited

Irina L. San Sebastián[1] · M. Gabriela Parisi[2,3] · Octavio M. Guilera[1,4] · Christos Efthymiopoulos[5]

Abstract

The aim of this paper is to provide an analytical tool, which might improve models in which the particle-in-a-box approach has been applied and that may be also used when the thin disk approximation could not be longer appropriate. The dispersion velocity is the root-mean-square planetesimal, asteroid, or Kuiper belt object velocity with respect to the local mean circular orbit. This velocity is a function of the object orbital eccentricity and inclination. We calculate a general expression of the dispersion velocity for the planar case in which the object's orbit has no inclination with respect to the local mean circular orbit and for the spatial case in which it has an inclined orbit. Our general expression of the square of the dispersion velocity may be expanded around any value of e for the planar and spatial cases, being in space an exact solution of the orbital inclination i. We expanded our expression around $e = 0$ with $i = e/2$ to study solid accretion rates and collision probabilities. We find that in the whole range of eccentricities and inclinations, our results are lower than solid accretion rates and collision probabilities computed by using the expressions of the dispersion velocity usually adopted in the literature. We apply our expressions of the square of the dispersion velocity expanded around $e=0$ and up to sixth order in e in our numerical model of planetary formation with planetesimal fragmentation and in our model of the collisional frequency on large asteroids. Our formalism, although generally giving lower values than previous approximations, validates the formerly used estimates for the applications presented here. In addition, we calculate the statistical velocity dispersion obtaining a straightforward expression as a function of the eccentricity.

✉ M. Gabriela Parisi
  gabriela_parisi@hotmail.com

1 Instituto de Astrofísica de La Plata, CONICET-UNLP, Paseo del Bosque s/n, 1900 La Plata, Buenos Aires, Argentina

2 Instituto Argentino de Radioastronomía, CONICET- CICPBA-UNLP, CC No. 5 Villa Elisa, Buenos Aires, Argentina

3 Facultad de Ciencias Astronómicas y Geofísicas, UNLP, Paseo del Bosque s/n, 1900 La Plata, Buenos Aires, Argentina

4 Grupo Milenio de Formación Planetaria (NPF), Avenida España 1680, 2340000 Valparaíso, Chile

5 Dipartimento di Matematica Tullio Levi-Civita, Universitá degli Studi di Padova, Via Trieste 63, 35121 Padova, Italy

1 Introduction

The particle-in-a-box approximation, first developed by Safronov (1972), has been the analytic approach for calculating the evolution of planetesimals, asteroid belt objects (ABs), and Kuiper belt objects (KBs) velocities when the number of objects is very large (Wetherill and Stewart 1993; Ida et al. 2008; Morbidelli et al. 2009; Weidenschilling 2011; Guilera et al. 2010, 2011, 2014; Chambers 2014; San Sebastián et al. 2019; Beitz et al. 2016). This approach approximates the relative orbital motions of the bodies with respect to the local mean circular orbit, with a dispersion velocity which is a function of their orbital eccentricity e and inclination i. The evolution of e and i is affected by several processes at different time stages for each scenario. For planetesimals, mainly it increases as a result of mutual perturbations among planetesimals and the stirring produced by the embryo and decreases by inelastic collisions, dynamical friction by smaller and leftover planetesimals (as well as the debris from the collisions between planetesimals and planetary embryos), gas dynamical friction and by gas drag (Inaba et al. 2001; Chambers 2006; Grishin and Perets 2015).

The best way to study planetesimals, ABs and KBs evolution, is via N-body simulations (Ida and Makino 1993; Ronco and de Elía 2018) since the dynamics, and therefore, the velocity dispersion of these objects is not affected only by the first body adjacent to them; it is affected by the entire population of the disk, i.e., the effect of the entire system should be included in the simulation at the same time. However, taking into account all the processes involved together is a very complicated task since N-body simulations when N is very large may take long calculation times.

In a series of previous works (Guilera et al. 2010, 2011, 2014), we developed a numerical model that describes the formation of giant planets immersed in a protoplanetary disk that evolves in time, where the gaseous component evolves by an exponential decay and planets grow by simultaneous accretion of solids and gas. The solid component of the disk evolves by planet accretion, radial drift due to nebular drag, and collisional evolution. During the planetary growth, collisional cascades of small fragments appear as a result of high impact velocity among planetesimals (Guilera et al. 2014; Chambers 2014). Our disk is divided into thin radial rings, where the particle-in-a-box approach at each ring is applied. Very recently, we improved our planetesimal fragmentation model developed in Guilera et al. (2014) incorporating several processes and different velocity regime models for the calculation of low and high relative planetesimal velocities (San Sebastián et al. 2019). We computed (San Sebastián et al. 2019) the solid accretion rate of a protoplanetary embryo considering three different regimes for the relative velocities and their transitions according to Greenberg et al. (1991), regime A: dominance by random motion (usually known as dispersion dominated regime); regime B: dominance by Keplerian shear motion; regime C: Keplerian shear dominance in a very thin disk. We found (San Sebastián et al. 2019) that planetesimal relative velocities are quickly increased due to the gravitational perturbations produced by the growing protoplanet leading to a rapid dominance of regime A. This suggests a revision of the usual expression of the dispersion velocity valid for larger values of the eccentricities and inclinations.

The conversions between orbital elements and relative velocities in the particle-in-a-box approximation assume $(e, i) << 1$ (Safronov 1972; Czechowski et al. 1992; Lissauer and Stewart 1993). The planetesimal dispersion velocity in the particle-in-a-box approach has

usually been adopted up to the present in the literature (Wetherill and Stewart 1993; Ida et al. 2008; Morbidelli et al. 2009; Weidenschilling 2011; Guilera et al. 2010, 2011, 2014; Chambers 2014; San Sebastián et al. 2019) and is the velocity of a planetesimal relative to the local mean circular orbit averaged over an epicycle and over a vertical oscillation (Lissauer and Stewart 1993).

There is a distinction between the cases in which eccentricities and inclinations may be damped during planet formation in the gas disk, and the gas-free case, when minor bodies are under study. In the gas-free case (ABs and KBs) eccentricities can grow large. There are also other problems in planetary science where a dynamical hot disk of planetesimals naturally appears, such as the formation of the Moon or the Uranian satellites, or the reaccumulation of material that could form binaries in asteroid collisions. Also, during the violent dynamical evolution of the giant planets orbits required by the so-called Nice Model (Tsiganis et al. 2005), a large number of primitive trans-Neptunian objects in elongated and inclined orbits are inserted into the inner Solar System (Gomes et al. 2005; Levison et al. 2009).

The formation and dynamical evolution of ABs and KBs is usually studied using the particle-in-a-box approximation, where the square velocity of a body relative to another body in the belt is taken as the sum of the square of the dispersion velocity of both objects (Stern 1996b, a; Stern and Colwell 1997; Bottke et al. 2005; Morbidelli et al. 2009; Weidenschilling 2011; Parisi 2013; Beitz et al. 2016; Parisi et al. 2016). We determined (Beitz et al. 2016; Parisi et al. 2016) the distribution of the present collision velocities of ABs from the orbital parameters of $\sim$ 500,000 asteroids with semiaxis between 2.2 and 3.75 AU provided by Chamberlin (2008) [1], where we computed the velocity-frequency distribution of the present ABs as the dispersion velocity using the particle-in-a-box approach, obtaining that the normalized accumulated asteroid number saturates at collision velocities of $\sim$ 10 km s^{-1} ($e \sim 0.5$).

In this paper, we calculate a general expression of the dispersion velocity that may be expanded around any value of the orbital eccentricity, which is an exact function of the orbital inclination. In Sect. 2, we present the basic equations of the intersection of an elliptical orbit with the local mean circular orbit. In Sect. 3, the general and complete expression of the dispersion velocity is calculated, where we compute the relative velocity of an object circulating the central star on an elliptical orbit with respect to the local mean circular orbit, for the planar and the spatial cases. The particular case of the statistical velocity dispersion, where the mean velocity of the object is equal to the local mean circular velocity for the planar and the spatial cases, is also calculated. In Sect. 4, we expand our expression of the square of the dispersion velocity around e=0 up to sixth order in e and is compared with the standard dispersion velocity usually used in the literature for the planar and spatial cases. The results and applications of Sect. 4 are shown in Sect. 5, where semianalytical results of accretion rates and collision probabilities are presented in Sect. 5.1, the calculation of the collision frequency on undifferentiated asteroids is presented in Sect. 5.2, and numerical results of giant planet formation including planetesimal fragmentation in a gaseous disk are shown in Sect. 5.3. Finally, the conclusions are presented in Sect. 6.

---

[1] http://ssd.jpl.nasa.gov/dat/ELEMENTS.NUMBR.

2 Intersection of an elliptical orbit around a central star with the local mean circular orbit

The basic equations of the orbits of a planetesimal and a protoplanet and their intersection are here presented, which are applied for the calculation of the dispersion velocity in Sect. 3. This mathematical formulation is also valid for the intersection of the orbits of ABs or KBs with the local mean circular orbit.

The equation that describes the elliptical orbit of a body of mass m around its central star is given by

$$R = \frac{a(1 - e^2)}{1 + e \cos \varphi}, \tag{1}$$

with R the radial distance of the body from its central star, φ and e the true anomaly and the eccentricity of the object's orbit, and a its semimajor axis. The radial and tangential components of the object's orbital velocity are (Murray and Dermott 1999):

$$\dot{R} = \frac{R^2 e \sin \varphi \dot{\varphi}}{a(1 - e^2)}, \tag{2}$$

$$R\dot{\varphi} = \frac{R^2(1 + e \cos \varphi)}{a(1 - e^2)} \dot{\varphi}. \tag{3}$$

The circular velocity v_0 of the protoplanet M or of the local mean circular orbit of radius a_0 is given by

$$v_0 = \sqrt{\frac{GM_*}{a_0}}, \tag{4}$$

being G the gravitational constant and M_* the central star mass.

In the intersection of the orbit of m with the local mean circular orbit, we have

$$a_0 = \frac{a(1 - e^2)}{1 + e \cos \varphi}, \tag{5}$$

where a may be expressed in the way defined by Czechowski et al. (1992) as a function of a_0

$$a = a_0(1 + \tilde{a}). \tag{6}$$

Substituting Eq. (6) into Eqs. (2) and (3), and using the second and the third Kepler's laws, we obtain

$$\dot{R} = \frac{v_0}{(1 + \tilde{a})^{1/2}} \frac{e \sin \varphi}{(1 - e^2)^{1/2}} \tag{7}$$

$$R\dot{\varphi} = \frac{v_0}{(1 + \tilde{a})^{1/2}} \frac{(1 + e \cos \varphi)}{(1 - e^2)^{1/2}}, \tag{8}$$

with the parameter $\tilde{a}$ obtained by using Eqs. (6) and (5)

$$\tilde{a} = \frac{e \cos \varphi + e^2}{1 - e^2}. \tag{9}$$

It should be noted that for the encounter to take place at $R = (a_0, \varphi)$, the object's semimajor axis cannot be independent from its eccentricity. If we fix its eccentricity, there is a unique a allowed, the one given by Eqs. (6) and (9).

3 Calculation of the dispersion velocity

The object's orbital velocity in cylindrical coordinates $\bar{V} = (V_R, V_\varphi, 0) = (\dot{R}, R\dot{\varphi}, 0)$ is expressed from Eqs. (7) and (8) as

$$\bar{V} = \frac{v_0}{(1 - e^2)^{1/2}(1 + \tilde{a})^{1/2}}(e \sin \varphi, 1 + e \cos \varphi, 0). \tag{10}$$

At the intersection of the orbits of m and M, substituting Eq. (9) into Eq. (10), we obtain

$$\bar{V} = \frac{v_0}{(1 + e \cos \varphi)^{1/2}}(e \sin \varphi, 1 + e \cos \varphi, 0). \tag{11}$$

3.1 Planar case

The square of the dispersion velocity between two bodies on co-planar elliptical orbits was calculated at second order by Czechowski et al. (1992). Following their procedure, we compute the general expression of the dispersion velocity, i.e., the root square of the mean square velocity v_{DP} of a body m relative to the coplanar circular orbit with radius a_0.

In computing the square of the dispersion velocity $v_{DP}^2 = \langle(\bar{V} - \bar{v}_0)^2\rangle$, we first calculate the square velocity of the planetesimal m relative to the circular orbital velocity of the protoplanet M.

From Eq. (11), and being $\bar{v}_0 = (0, v_0, 0)$ the protoplanet coplanar circular velocity in cylindrical coordinates, we get

$$(\bar{V} - \bar{v}_0)^2 = v_0^2 \left[\frac{e^2 \sin^2 \varphi}{1 + e \cos \varphi} + \left((1 + e \cos \varphi)^{1/2} - 1\right)^2 \right]. \tag{12}$$

Since, for the encounter to occur, the planetesimal's orbit is determined by Eq. (9), the planetesimal semimajor axis is not independent of its eccentricity. Therefore, the average of $\langle(\bar{V} - \bar{v}_0)^2\rangle$ over one orbital period is carried out as Safronov (1972)

$$< (\bar{V} - \bar{v}_0)^2 > = \frac{1}{2\pi} \int_0^{2\pi} (\bar{V} - \bar{v}_0)^2 \, d\varphi. \tag{13}$$

Then, following Eq. (13), we average Eq. (12)

$$v_{DP}^2 = \langle(\bar{V} - \bar{v}_0)^2\rangle = v_0^2 \left[\left\langle \frac{e^2 \sin^2 \varphi}{1 + e \cos \varphi} \right\rangle \right]$$
$$+ v_0^2 \left[\langle((1 + e \cos \varphi)^{1/2} - 1)^2\rangle \right], \tag{14}$$

where

$$\left\langle \frac{e^2 \sin^2 \varphi}{1 + e \cos \varphi} \right\rangle = \left[1 - (1 - e^2)^{1/2} \right], \tag{15}$$

and

$$\langle((1 + e \cos \varphi)^{1/2} - 1)^2\rangle = 2 - 2\langle(1 + e \cos \varphi)^{1/2}\rangle, \tag{16}$$

with

$$\langle(1 + e \cos \varphi)^{1/2}\rangle$$
$$= \left[\frac{1}{\pi}(1 - e)^{1/2} E \left(\frac{2e}{-1 + e} \right) + \frac{1}{\pi}(1 + e)^{1/2} E \left(\frac{2e}{1 + e} \right) \right], \tag{17}$$
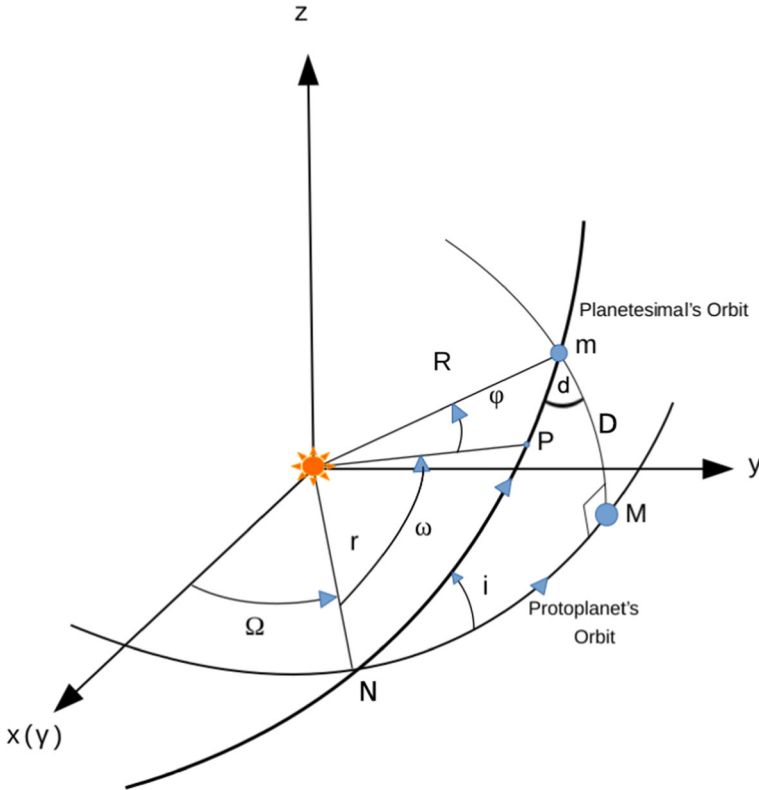
Fig. 1 The orbital configuration diagram in space. The reference frame is centered at the star and the x-axis points in the direction of the vernal equinox. The circular orbit of the protoplanet M is in the (x, y) plane. R is the distance between the planetesimal m and the central star, i is the inclination of the planetesimal's orbit with respect to the protoplanet's orbital plane. r is the distance between the node N and the central star ($r = a_0$). P is the orbital pericenter of m. The angles Ω, ω and φ are the longitude of the ascending node, the longitude of the pericenter and the true anomaly, respectively

being E the complete elliptic integral of the second kind. Substituting Eqs. (15), (16), and (17) in Eq. (14), the two-dimensional square dispersion velocity v_{DP}^2 is obtained:

$$v_{DP}^2 = v_0^2 \left[(3 - (1 - e^2)^{1/2}) \right]$$
$$- v_0^2 \left[\frac{2}{\pi} (1 - e)^{1/2} E \left(\frac{2e}{-1 + e} \right) + \frac{2}{\pi} (1 + e)^{1/2} E \left(\frac{2e}{1 + e} \right) \right]. \tag{18}$$

Expanding Eq. (18) around $e = 0$, we get

$$v_{DP}^2 = v_0^2 \left(\frac{5}{8} e^2 + \frac{79}{512} e^4 + \frac{617}{8192} e^6 + \ldots \right). \tag{19}$$

This same result may be found from the restricted three-body problem (Danby 1992; Kaula 1968) for orbital inclination $i = 0^o$ (see app. A.0.1).

3.2 Spatial case

We compute the spatial dispersion velocity, i.e., the root square of the mean square velocity v_{DS} of a planetesimal m in elliptical orbit relative to the circular orbit with radius a_0 of a protoplanet M, where the orbital planes of M and m are separated by an inclination i. The elliptical and circular orbits of m and M are shown in Fig. 1, where Ω, ω, and φ, are the longitude of the ascending node, the longitude of the pericenter and the true anomaly. This procedure is also valid for the elliptical orbit of ABs and KBs intersecting the local mean circular orbit.

Following (Adachi et al. 1976), we measure the orbital velocities of the planetesimal and the planet in cylindrical coordinates in the heliocentric planetesimal orbital system. Then, the orbital velocity of m is $\bar{V}$ given by Eq. (11), while from Fig. 1, the orbital velocity of M in cylindrical coordinates is:

$$\bar{v}_{0S} = (0, v_0 \sin d, -v_0 \cos d). \tag{20}$$

The square of the relative velocity is then given by

$$(\bar{V} - \bar{v}_{0S})^2 = v_0^2 \left[\frac{e^2 \sin^2 \varphi}{1 + e \cos \varphi} + ((1 + e \cos \varphi)^{1/2} - \sin d)^2 + \cos^2 d \right]. \tag{21}$$

We average Eq. (21), following Eq. (13), over one orbital period

$$v_{DS}^2 = \langle (\bar{V} - \bar{v}_{0S})^2 \rangle = v_0^2 \left[\left\langle \frac{e^2 \sin^2 \varphi}{1 + e \cos \varphi} \right\rangle \right]$$
$$+ v_0^2 \left[\langle ((1 + e \cos \varphi)^{1/2} - \sin d)^2 + \cos^2 d \rangle \right], \tag{22}$$

where d is obtained from Napier's rules for right spherical triangles (Adachi et al. 1976) from the triangle NmM of Fig. 1

$$\sin d = \frac{\cos i}{\cos D}, \tag{23}$$

with

$$\cos D = \frac{a_0}{R}. \tag{24}$$

Substituting Eq. (15) in the first term of the right hand of Eq. (22) and developing the second term of Eq.(22), v_{DS}^2 is obtained using Eqs. (23) and (24), and substituting Eqs.(1), (6) and (9)

$$v_{DS}^2 = v_0^2 \left[(3 - (1 - e^2)^{1/2}) \right] - 2v_0^2 \cos i \left\langle (1 + e \cos \varphi)^{1/2} \right\rangle, \tag{25}$$

with $\langle (1 + e \cos \varphi)^{1/2} \rangle$ given by Eq. (17).

Equation (25) is general and complete and may be expanded around any value of e being an exact solution of the orbital inclination i.

Expanding Eq. (25) around $e = 0$, we get

$$v_{DS}^2 = v_0^2 \left[2 - 2 \cos i + e^2 \left(\frac{1}{2} + \frac{1}{8} \cos i \right) \right]$$
$$+ v_0^2 \left[e^4 \left(\frac{1}{8} + \frac{15}{512} \cos i \right) + e^6 \left(\frac{1}{16} + \frac{105}{8192} \cos i \right) + ... \right]. \tag{26}$$

Note that when $i = 0^o$, $v_{DS}^2 = v_{DP}^2$. The result of Eq. (25) may be also found from the restricted three-body problem (Danby 1992; Kaula 1968) (see app. A.0.2).

3.3 Particular case: statistical velocity dispersion

The statistical dispersion of velocities about the mean velocity is usually called the statistical velocity dispersion σ. For the case in which the dispersion velocity is the statistical dispersion of velocities, the mean velocity of the planetesimal is equal to the circular Keplerian velocity of the protoplanet.

For the planar case, $\langle \bar{V} \rangle = \bar{v}_0$. Then, $v_{DP} = \sigma_p$ and the following equality is fulfilled

$$\sigma_p^2 = \langle (\bar{V} - \bar{v}_0)^2 \rangle = \langle \bar{V}^2 \rangle - \langle \bar{v}_0^2 \rangle, \tag{27}$$

arriving to

$$\sigma_p^2 = \langle \bar{V}^2 \rangle - v_0^2 = v_0^2 (1 - (1 - e^2)^{1/2}). \tag{28}$$

Note that when $e = 0$, $\sigma_p = 0$ while if $e = 1$, $\sigma_p = v_0$.

For the spatial case, $\langle \bar{V} \rangle = \bar{v}_{0S}$. Then $v_{DS} = \sigma_S$ and the following equality is fulfilled

$$\sigma_S^2 = \langle (\bar{V} - \bar{v}_{0S})^2 \rangle = \langle \bar{V}^2 \rangle - \langle \bar{v}_{0S}^2 \rangle, \tag{29}$$

arriving to

$$\sigma_S^2 = \langle \bar{V}^2 \rangle - v_{0S}^2 = v_0^2 (1 - (1 - e^2)^{1/2}). \tag{30}$$

If $e = 0$, $\sigma_S = \sigma_p = 0$ while if $e = 1$, $\sigma_S = \sigma_p = v_0$. Then $\sigma_S^2 = \sigma_p^2$.

4 Comparison with the standard dispersion velocity

The usual conversions between orbital elements and relative velocities assume $e << 1$ for the planar case (Czechowski et al. 1992; Lissauer and Stewart 1993; Safronov 1972) and (e, i) $<< 1$ for the spatial case (Lissauer and Stewart 1993). In the following, we define standard dispersion velocity v_{2std} (v_{3std}) for the planar (spatial) case, to the planetesimal dispersion velocity defined by Lissauer and Stewart (1993), which has been up to the present usually adopted in the literature (Guilera et al. 2010, 2011, 2014; Ida et al. 2008; Morbidelli et al. 2009; Weidenschilling 2011; Wetherill and Stewart 1993; Chambers 2014; San Sebastián et al. 2019).

4.1 Planar case

We call standard dispersion velocity v_{2std} to the velocity of a planetesimal relative to the local mean circular orbit averaged over an epicycle, which was given by Lissauer and Stewart (1993) and calculated by Czechowski et al. (1992) and (Safronov 1972)

$$v_{2std} = v_0 \left(\frac{5}{8} e^2 \right)^{\frac{1}{2}}. \tag{31}$$

Note that v_{DP}^2 given by Eq. (18) and expanded around $e = 0$ (Eq. (19)) up to second order in e is equal to the square of the standard dispersion velocity v_{2std}^2. The results of Eq. (19) up to fourth and sixth order in e, i.e., $v_{DP(4th)}^2$ and $v_{DP(6th)}^2$, are shown in Fig. 2 (left), where v_{2std}^2 is also shown for comparison.

In Table 1, we show the differences between our calculation of the dispersion velocity and the standard expression, i.e., $\left(\sqrt{v_{DP(4th)}^2} - v_{2std} \right)$ and $\left(\sqrt{v_{DP(6th)}^2} - v_{2std} \right)$. We can

Table 1 Difference between our results of the dispersion velocity and the standard one for the planar case expressed in m s^{-1}. The square of the dispersion velocity is calculated up to fourth ($v_{DP(4th)}^2$) and up to sixth ($v_{DP(6th)}^2$) order. v_o is the local circular velocity in m s^{-1} with semiaxis a_o in AU, and e is the planetesimal orbital eccentricity

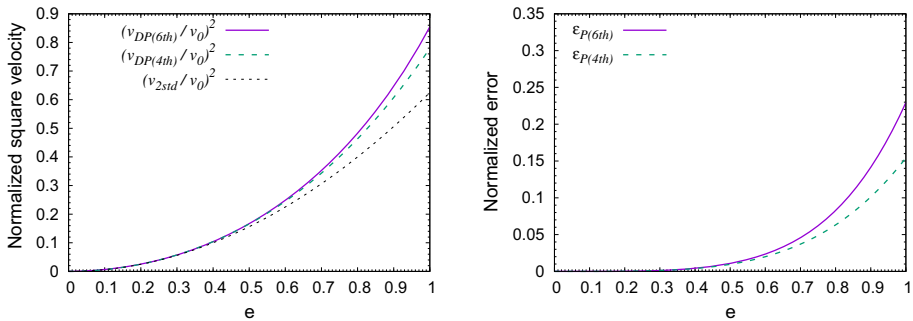| e	a_o [AU]	v_o [ms^{-1}]	$\sqrt{v_{DP(4th)}^2} - v_{2std}$ [ms^{-1}]	$\sqrt{v_{DP(6th)}^2} - v_{2std}$ [ms^{-1}]
0.2	1	29788	23.20	23.66
	3	17198	13.39	13.65
	5	13322	10.37	10.58
	30	5439	4.24	4.32
0.4	1	29788	184.24	198.55
	3	17198	106.37	114.60
	5	13322	82.39	88.77
	30	5439	33.64	36.24
0.7	1	29788	968.93	1192.82
	3	17198	559.22	688.44
	5	13322	433.19	533.28
	30	5439	176.86	217.72
0.9	1	29788	2023.29	2638.79
	3	17198	1167.75	1522.98
	5	13322	904.57	1180.36
	30	5439	369.31	481.90

Fig. 2 Planar Case. Left: Normalized square of the dispersion velocity as a function of the planetesimal's orbital eccentricity e up to sixth order ($v_{DP(6th)}^2$, full line) and up to fourth order ($v_{DP(4th)}^2$, long dashed line). The square of the standard dispersion velocity v_{2std}^2 is shown in short dashed line. Right: The normalized error ϵ_p as a function of e with the square of the dispersion velocity at sixth order ($\epsilon_{p(6th)}$, full line) and at fourth order (ϵ_p(4th), long dashed line)

see that the differences increase with the inclusion of higher-order terms as well as with the eccentricity and decrease with a_o. The differences shown in Table 1 might be significant for $e \geq 0.4$.

We define the normalized error ϵ_p as

$$\epsilon_p = \frac{|v_{DP}^2 - v_{2std}^2|}{v_0^2}. \tag{32}$$

The error given by Eq. (32) with Eq. (19) up to fourth order ($\epsilon_{p(4th)}$) and up to sixth order ($\epsilon_{p(6th)}$) is shown in Fig. 2 (right).
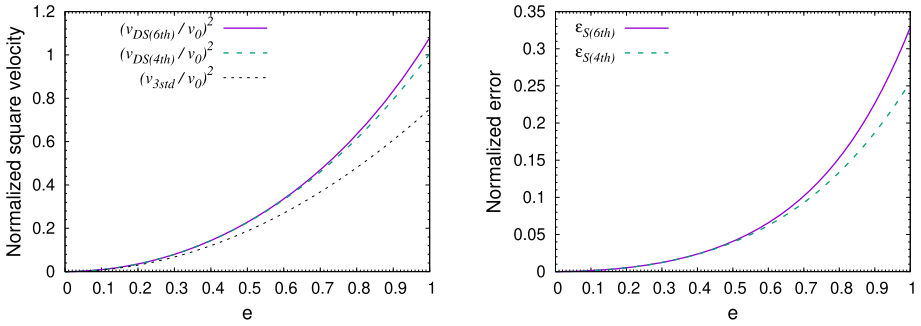
Fig. 3 Spatial case. Left: Normalized square of the dispersion velocity as a function of the planetesimal's orbital eccentricity e up to sixth order in e ($v^2_{DS(6th)}$, full line) and up to fourth order ($v^2_{DS(4th)}$, long dashed line). The square of the standard dispersion velocity v^2_{3std} is shown in short dashed line. Right: The normalized error ϵ_s as a function of e with the square of the dispersion velocity at sixth order in e ($\epsilon_{s(6th)}$, full line) and at fourth order ($\epsilon_s(4th)$, long dashed line). In all cases we assume i=e/2

For $e = 0.2$, $\epsilon_{p(4th)}$ is 9.875 x 10^{-3} and $\epsilon_{p(6th)}$ is 1.0 x 10^{-2} while for $e \geq 0.4$, the inclusion of higher-order terms are not negligible since $\epsilon_{p(4th)}$ is 3.95 x 10^{-2} and $\epsilon_{p(6th)}$ 4.26 x 10^{-2}.

4.2 Spatial case

We call standard dispersion velocity v_{3std} to the dispersion velocity given by Lissauer and Stewart (1993), which has been up to the present usually adopted in the literature (Guilera et al. 2010, 2011, 2014; Ida et al. 2008; Morbidelli et al. 2009; Weidenschilling 2011; Wetherill and Stewart 1993; San Sebastián et al. 2019), and is the velocity of a planetesimal relative to the local mean circular orbit averaged over an epicycle and over a vertical oscillation assuming $\sin i \sim i$ (See app. B)

$$v_{3std} = v_0 \left(\frac{5}{8}e^2 + \frac{1}{2}i^2 \right)^{\frac{1}{2}}. \tag{33}$$

The results of Eq. (26) up to fourth and sixth order in e, i.e., $v^2_{DS(4th)}$ and $v^2_{DS(6th)}$, are shown in Fig. 3 (left), where v^2_{3std} is also shown for comparison. We have assumed $\cos i = \cos(e/2)$ (San Sebastián et al. 2019) to plot Fig. 3.

In the same way as for the planar case, we define the normalized error ϵ_s as

$$\epsilon_s = \frac{|v^2_{DS} - v^2_{3std}|}{v^2_0}. \tag{34}$$

The error given by Eq. (34) with the square of the dispersion velocity up to fourth order ($\epsilon_{s(4th)}$) and up to sixth order ($\epsilon_{s(6th)}$) in e is shown in Fig. 3 (right). For $e = 0.4$, ($\sqrt{v^2_{DS(6th)}} - v_{3std}$) is $\sim 0.03v_0$, while for $e = 0.8$, ($\sqrt{v^2_{DS(6th)}} - v_{3std}$) is $\sim 0.1v_0$.

In Table 2, we present the summary of the planetesimal dispersion velocities presented in this paper.

Table 2 Summary of the square of dispersion velocities

Planar case	
Dispersion velocity	$v_{DP}^2 = v_0^2 \left[(3 - (1 - e^2)^{1/2}) \right]$
	$-v_0^2 \left[\frac{2}{\pi}(1 - e)^{1/2} E\left(\frac{2e}{-1+e}\right) + \frac{2}{\pi}(1 + e)^{1/2} E\left(\frac{2e}{1+e}\right) \right]$
Dispersion velocity (6th)	$v_{DP(6th)}^2 = v_0^2 \left(\frac{5}{8}e^2 + \frac{79}{512}e^4 + \frac{617}{8192}e^6 \right)$
Statistical velocity dispersion	$\sigma_p^2 = v_0^2(1 - (1 - e^2)^{1/2})$
Standard dispersion velocity	$v_{2std}^2 = v_0^2 \left(\frac{5}{8}e^2 \right)$
Spatial case	
Dispersion velocity	$v_{DS}^2 = v_0^2 \left[(3 - (1 - e^2)^{1/2}) \right]$
	$-v_0^2 \cos i \left[\frac{2}{\pi}(1 - e)^{1/2} E\left(\frac{2e}{-1+e}\right) + \frac{2}{\pi}(1 + e)^{1/2} E\left(\frac{2e}{1+e}\right) \right]$
Dispersion velocity (6th)	$v_{DS(6th)}^2 = v_0^2 \left[2 - 2\cos i + e^2(\frac{1}{2} + \frac{1}{8}\cos i) \right] + v_0^2$
	$\left[e^4(\frac{1}{8} + \frac{15}{512}\cos i) + e^6(\frac{1}{16} + \frac{105}{8192}\cos i) \right]$
Statistical Velocity Dispersion	$\sigma_S^2 = v_0^2(1 - (1 - e^2)^{1/2})$
Standard Dispersion Velocity	$v_{3std}^2 = v_0^2 \left(\frac{5}{8}e^2 + \frac{1}{2}i^2 \right)$

5 Results and applications

We apply the expansion of Eq. (25) around $e = 0$ (Eq. (26)) up to sixth order in e to study on one hand, semianalytical approaches (Sect. 5.1) and the collision frequency on large asteroids (Sect. 5.2) in a gas-free enviroment, and on the other hand, the formation of a giant planet including planetesimal fragmentation in a gaseous disk (Sect. 5.3).

5.1 Semianalytical calculations

5.1.1 Accretion rates

It was shown that dispersion velocities are a key factor in the solid accretion rate of protoplanets (Guilera et al. 2010, 2014; Chambers 2006, 2014; Inaba et al. 2001; San Sebastián et al. 2019). We compute a very simple calculation of solid accretion rates in a gas-free environment in order to evaluate the behavior of accretion rates when our calculation of the dispersion velocity is applied. In a more realistic model of planetary formation, gas is still present; thus, the eccentricities and inclinations may not be excited to too large values since they are obtained as an equilibrium between the damping effects of the gas drag and the dynamical stirring of the planetesimal population (Chambers 2006; San Sebastián et al. 2019). A more elaborated model of planetesimal accretion (Inaba et al. 2001; San Sebastián et al. 2019) is presented in Sect. 5.3. The simple and easy form of the solid accretion rate $\dot{M}$ of a terrestrial protoplanet or of the core of a giant planet is (Lissauer and Stewart 1993)

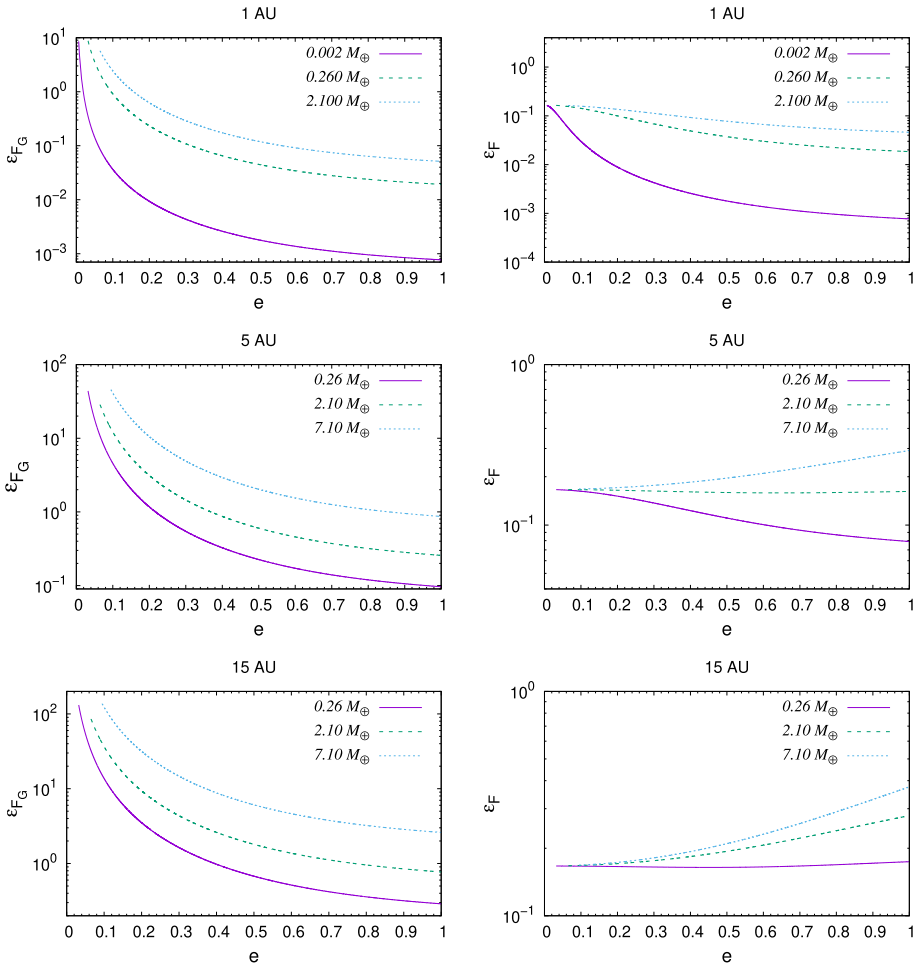$$\dot{M} = \frac{2\sqrt{3}\pi^2 \Sigma(a_0) R_C^2 F_{Gstd}}{2 P_M},$$ (35)

Fig. 4 Error in the focusing factor ϵ_{FG} (left panel) and relative error ϵ_F (right panel) as a function of e for $e > e_{min}$. Top: $a_0 = 1$ AU and M= 0.002, 0.260 and 2.100 $M_\oplus$. Middle: $a_0 = 5$ AU and M= 0.260, 2.100 and 7.10 $M_\oplus$. Bottom: $a_0 = 15$ AU and M= 0.260, 2.100 and 7.10 $M_\oplus$. M and its corresponding e_{min} are taken from Table 3. In computing ϵ_{FG} and ϵ_F, v_{DS}^2 is taken up to sixth order in e ($v_{DS(6th)}^2$) with i=e/2

where $\Sigma(a_0)$ is the surface mass density distribution of planetesimals at a distance a_0 from the central star M_*, R_C is the radius of M and P_M is the period of its circular orbit with semiaxis a_0. The gravitational enhancement factor F_{Gstd} is Lissauer and Stewart (1993)

$$F_{Gstd} = \left(1 + \frac{v_e^2}{v_{3std}^2}\right), \tag{36}$$

with v_{3std}^2 given by Eq. (33) being v_e the escape velocity at the surface of M. As planetesimal velocities decrease, the gravitational enhancement factor increases to approximately twice the two-body value, and then, the gravitational effect of M_* should be taken into account (Greenzweig and Lissauer 1990). However, in the high-velocity regime, the gravitational focusing is well approximated by the two-body particle in a box approximation given by

Table 3 Our results of the minimum planetesimal orbital eccentricity e_{min} for which the dispersion dominated regime is valid and the minimum planetesimal orbital eccentricity e_{std} for which the high-velocity regime are valid

$R_c [Km]$	1×10^3	5×10^3	1×10^4	1.5×10^4
$M \, [M_\oplus]$	0.002	0.260	2.100	7.100
e_{std}	0.005	0.026	0.051	0.077
e_{min}	0.006	0.032	0.065	0.095

The results are shown for a protoplanet of mass M and radius R_C with a bulk density of 3 gr cm^{-3}

Eq. (36) where the gravitational effect of M_* is neglected (Greenzweig and Lissauer 1990; Lissauer and Stewart 1993). The high velocity regime is valid when the Hill eccentricity $e_H \geq 4$ and the Hill inclination $i_H \geq 2$ (Greenzweig and Lissauer 1990; Guilera et al. 2010; Inaba et al. 2001), where $e_H = e/H$ and $i_H = i/H$, with $H = R_H/a_0$ being R_H the protoplanet's Hill sphere. The minimum values of e, that we call e_{std}, for which the high velocity regime is valid (e_{std}=4 H) are shown in Table 3 for M = 0.002, 0.026, 2.1 and 7.1 $M_\oplus$ assuming $M_*=M_\odot$. In computing R_C, which is also shown in Table 3, a protoplanet bulk density ρ of 3 gr cm^{-3} is taken.

In a previous paper, we computed the minimum eccentricity e_{min} for which the dispersion dominated regime is valid (see our Appendix B.1 in San Sebastián et al. (2019) where we follow (Greenberg et al. 1991)). For a planetesimal with orbital semiaxis a, it satisfies

$$\frac{(a + a_0)e_{min}}{4} = 2.5Ha_0. \tag{37}$$

Substituting the average of Eq. (9) into Eq. (6), and Eq. (6) into Eq. (37), the following third-order equation is obtained

$$e_{min}^3 - 10He_{min}^2 - 2e_{min} + 10H = 0. \tag{38}$$

Equation (38) has three real solutions but only one root satisfies $0 < e_{min} < 1$, which is tabulated in Table 3.

From our general expression of the square of the spatial dispersion velocity given by Eqs. (25) and (26), the gravitational focusing factor F_G for $e > e_{min}$ is expressed in the following form:

$$F_G = \left(1 + \frac{v_e^2}{v_{DS}^2}\right). \tag{39}$$

Subtracting Eqs. (36) and (39), we define the error ϵ_{FG} in the focusing factor

$$\epsilon_{FG} = F_{Gstd} - F_G, \tag{40}$$

and the relative error ϵ_F

$$\epsilon_F = \frac{F_{Gstd} - F_G}{F_G}. \tag{41}$$

The results of ϵ_{FG} and ϵ_F as a function of e for $e > e_{min}$ are shown in Fig. 4 for three values of a_0 of 1, 5 and 15 AU. Note that Eq. (26) depends on a_0 through v_0 (Eq. (4)). For each a_0, three values of M and its corresponding e_{min} are taken from Table 3. In computing Eqs.(40) and (41), v_{DS}^2 given by Eq. (26) is taken up to sixth order in e ($v_{DS(6th)}^2$) and assuming $i = e/2$ (San Sebastián et al. 2019).

Since the accretion rate is proportional to the gravitational focusing factor, we can see from Fig. 4 that our results of the accretion rate $\dot{M}$ result lower than previous calculations.

Note that after a number N of time steps δt in the calculation of the growth of a terrestrial planet or of the core of a giant planet, the accumulative error in M would become proportional to ($N \epsilon_{FG}$).

Our results of ϵ_F show that the focusing factor given by Eq. (39) with v_{DS}^2 up to sixth order in e ($v_{DS(6th)}^2$) reduces $\dot{M}$ such that for low e, ϵ_F saturates at 0.166. Then, our calculation of solid accretion rates are lower than former calculations being at most $\sim$ 86 per cent of the previous estimates for low e. It means that by using our improved equations, we get differences with respect to the previous equations, even for low e. It should be noted that ϵ_F increases with M and a_0. For M= 7 $M_\oplus$ and a_0 = 5 AU (15 AU) $\epsilon_F \sim$ 0.3 (0.4) for high eccentricities. Our results of solid accretion rates are then at most $\sim$ 70 per cent of the previous estimates for high e. Although ϵ_F would be reduced when gas is present (Chambers 2006), we will see in Sect. 5.3 that the protoplanet achieves the crossover mass at a longer time than our previous simulations where the standard dispersion velocity usually adopted in the literature has been applied (San Sebastián et al. 2019).

5.1.2 Collision probabilities

We are interested in the behavior of collision probabilities among minor bodies when our calculation of the dispersion velocity is applied. The dispersion velocity plays an important role in calculations of the collisional evolution of ABs (see Sect. 5.2) and KBs, where collisions may be destructive (Beitz et al. 2016; Morbidelli et al. 2009; Parisi 2013; Parisi et al. 2016; Stern and Colwell 1997). It also plays a role in the probability collision among planetesimals in models of planetary formation including planetesimal fragmentation (see Sect. 5.3).

The total number of collisions between projectiles p and targets T in a time step δt is given by Morbidelli et al. (2009); San Sebastián et al. (2019); Wetherill and Stewart (1993)

$$N_{Cstd}(p, T) = P_{Istd}(p, T) N_p N_T F_{Gstd}(p, T) \pi (R_p + R_T)^2 \delta t, \qquad (42)$$

where $P_{Istd}(p.T)$ is the intrinsic collision probability, N_p and N_T are the number of particles p and T contained in the volume Vol_{std}, R_p and R_T are the radii of the particles p and T, and $F_{Gstd}(p, T)$ is the gravitational focusing factor. In the high-velocity regime, $F_{Gstd}(p, T)$ is given by

$$F_{Gstd}(p, T) = \left(1 + \frac{v_e^2(p, T)}{v_{3std}^2(p, T)}\right), \qquad (43)$$

being $v_e(p, T) = \sqrt{2G(M_p + M_T)/(R_p + R_T)}$ the mutual escape velocity between the projectile with mass M_p and the target with mass M_T at the point of contact. The square of the relative velocity $v_{3std}^2(p, T) = v_{3std}^2(p) + v_{3std}^2(T)$, where $v_{3std}^2(p)$ and $v_{3std}^2(T)$ are given by Eq. (33) for the projectile and target eccentricities and inclinations (e_p, i_p) and (e_T, i_T), respectively. It should be mentioned that in computing $v_{3std}^2(T)$ and $v_{3std}^2(p)$ from Eq. (33), Morbidelli et al. (2009) take $\sin i_T$ and $\sin i_p$ without approaching $\sin i \sim i$ (See app. B).

The intrinsic collision probability is expressed in the following form Morbidelli et al. (2009); San Sebastián et al. (2019); Wetherill and Stewart (1993)

$$P_{Istd}(p, T) = \frac{\alpha v_{3std}(p, T)}{Vol_{std}}, \qquad (44)$$

where α=0.855 in the high-velocity regime and the volume Vol_{std} is given at first order by Morbidelli et al. (2009)

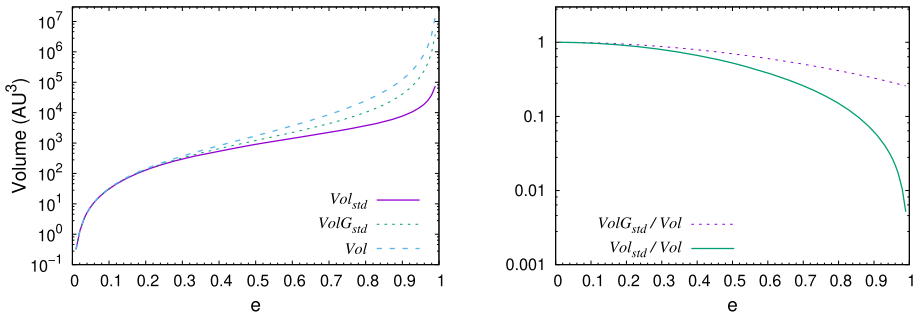$$Vol_{std} = 4\pi H_c a_0 (\Delta a + 2a_0 e). \qquad (45)$$

Fig. 5 Left: Comparison between the volume at first order Vol_{std} (full line), the complete expression of the volume $VolG_{std}$ (dotted line) and our exact calculation of the volume Vol (dashed line) with $a_0 = 5$ AU. Right: Ratios of Vol_{std} (full line) and $VolG_{std}$ (dotted line) over our exact calculation of the volume Vol. We take $e_T = i_T = 0$, $e_p = e$, $i_p = i = e/2$. In computing Vol_{std} and $VolG_{std}$ we take $\Delta a = a_{Max} - a_{min}$

In Eq. (45), Δa is the total width of the annulus, which is usually taken as an ad hoc parameter, e is the mean eccentricity of the projectiles in the bin Δa, and H_c is the symmetrical mutual scale height

$$H_c = a_0\sqrt{sin^2 i_p + sin^2 i_T}. \tag{46}$$

We define the volume $VolG_{std} = 2H_c\pi(R^2_{extG} - R^2_{intG})$ where $R_{extG} = (a_0 + \Delta a/2)(1+e)$ and $R_{intG} = (a_0 - \Delta a/2)(1-e)$ in order to calculate the general expression of Eq. (45), obtaining

$$VolG_{std} = 4\pi H_c a_0(\Delta a + 2a_0 e + \Delta a e^2 + \Delta a^2 e/2a_0). \tag{47}$$

We can see that Eq. (47) at first order in Δa and e arrives to Eq. (45).

We obtain an expression of the volume for non-arbitrary values of the total width of the annulus, computing the volume $Vol = 2H_c\pi(R^2_{ext} - R^2_{int})$, where $R_{ext} = a_{Max}(1+e)$, and $R_{int} = a_{min}(1-e)$. From Eq. (6), $a_{Max} = a_0(1+\tilde{a}_{Max})$ and $a_{min} = a_0(1+\tilde{a}_{min})$. The values of $\tilde{a}_{Max}$ and $\tilde{a}_{min}$ are obtained from Eq. (9) setting $\varphi = 0$ and $\varphi = \pi$, respectively. Then, the exact expression of the volume gives

$$Vol = 2H_c\pi a_0^2\left[\frac{(1+e)^2}{(1-e)^2} - \frac{(1-e)^2}{(1+e)^2}\right]. \tag{48}$$

In the left panel of Fig. 5, we compare the different calculations for the volume Vol_{std}, $VolG_{std}$ and Vol at $a_0 = 5AU$. We can see that for low values of the eccentricity, the volumes are similar, while for high values of the eccentricity, the differences increase between one and two orders of magnitude. The ratio of Eqs. (45) and (48) (Vol_{std}/Vol) and of Eqs. (47) and (48) ($VolG_{std}/Vol$) are shown in Fig. 5 right, which result independent of a_0. We can see that $Vol_{std} < VolG_{std} < Vol$ and that the differences increase with e. In computing the results of Fig. 5, we take $\Delta a = a_{Max} - a_{min}$, $e_T = i_T = 0$, $e_p = e$, and $i_p = i = e/2$.

We can see from Eq. (42) that $N_{Cstd}(p, T)$ depends on $v_{3std}(p, T)$ through the $Factor_{std}(p, T)$ here defined in

$$Factor_{std}(p, T) = P_{Istd}(p, T)F_{Gstd}(p, T). \tag{49}$$

Fig. 6 Relative error $\epsilon_{NcR}(p,T)$ in the rate of impacts as a function of e assuming $M_T = M$ (with $M_p << M$) for $a_0 = 5$ AU with $M = 2.1 M_\oplus$. We take $e_T = i_T = 0$, $e_p = e$, and $i_p = i = e/2$. In computing $\epsilon_{NcR(p,T)}$, v_{DS}^2 is expanded around $e = 0$ and taken up to sixth order in e ($v_{DS(6th)}^2$). Solid line: $\epsilon_{NcR}(p,T)$ is calculated assuming $Volume = Vol$. Dashed line: $\epsilon_{NcR}(p,T)$ is calculated assuming $Volume = VolG_{std}$
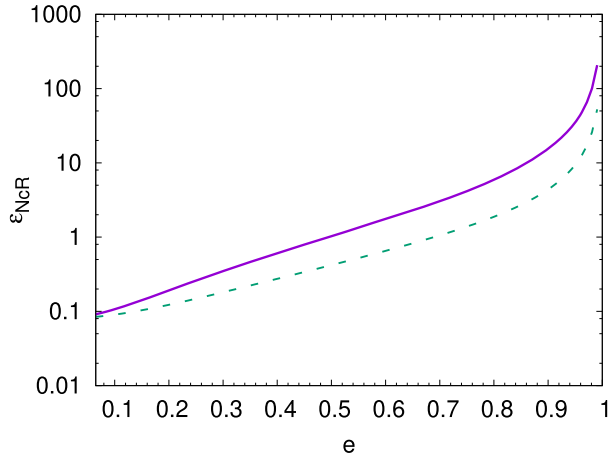
The general expression of the intrinsic collision probability $P_I(p.T)$ is:

$$P_I(p, T) = \frac{\alpha v_{DS}(p, T)}{Volume}, \tag{50}$$

being $v_{DS}^2(p, T)$ the square of the relative velocity $v_{DS}^2(p, T) = v_{DS}^2(p) + v_{DS}^2(T)$, where $v_{DS}^2(p)$ and $v_{DS}^2(T)$ are given by Eqs. (25) or (26) for the projectile and target eccentricities and inclinations (e_p, i_p) and (e_T, i_T), respectively, and $Volume$ can be taken as Vol or $VolG_{std}$.

We then define $Factor(p, T)$ as

$$Factor(p, T) = P_I(p, T)F_G(p, T), \tag{51}$$

where $F_G(p, T)$ is our calculations of the gravitational focusing factor in the high-velocity regime

$$F_G(p, T) = \left(1 + \frac{v_e^2(p, T)}{v_{DS}^2(p, T)}\right). \tag{52}$$

Subtracting Eqs. (49) and (51), we define the error ϵ_{Nc} in the number of collisions between projectiles p and targets T

$$\epsilon_{Nc}(p, T) = P_{Istd}(p, T)F_{Gstd}(p, T) - P_I(p, T)F_G(p, T). \tag{53}$$

In order to find a comparative error in the number of impacts, we here define the relative error $\epsilon_{NcR(p,T)}$ as

$$\epsilon_{NcR(p,T)} = \frac{Factor_{std}(p, T) - Factor(p, T)}{Factor(p, T)}. \tag{54}$$

In Fig. 6, the relative error $\epsilon_{NcR(p,T)}$ is shown for $a_0 = 5$ AU and $M = 2.1 M_\oplus$. For different values of a_0 and M, $\epsilon_{NcR(p,T)}$ has a similar behavior than in Fig. 6. We assume $e_T = i_T = 0$, $e_p = e$ with e > e_{min}, $i_p = i = e/2$, and $M_T = M$ (with $M_p << M$). In Fig. 6, v_{DS}^2 is computed through Eq. (25) expanded around $e = 0$ (Eq. (26)) and taken up to sixth order in e assuming $i = e/2$ ($v_{DS(6th)}^2$). We can see from Fig. 6 that the relative error in the number of impacts starts being ~ 10 per cent for low eccentricities and increases with increasing

e. In all cases, our results of the collision probabilities are lower than previous calculations (Morbidelli et al. 2009; San Sebastián et al. 2019).

5.2 Collision frequency on undifferentiated asteroids

In a previous work (Beitz et al. 2016; Parisi et al. 2016), we computed the number of collisions on a target of radius 100 km with projectiles of radius r during the age of the Solar System, where the usual expressions of the dispersion velocity were applied. Only impactors in the asteroid belt (AB) that are not rapidly removed by Yarkovsky effect ($r > 0.1$ m) and that do not lead to catastrophic disruption of the target ($r < 22$ km) (Jutzi et al. 2010; Parisi 2013) were considered.

Primordial large porous objects are subject to hydrostatic compression in their interiors that lead to a compaction of material and thus, to a density increase toward the center. The hydrostatic pressure P_h in the center of a body with radius R and mass M is given by Beitz et al. (2016)

$$P_h = \frac{3GM^2}{8\pi R^4}, \tag{55}$$

with G being the gravitational constant. If the compressional strength of the material, p_{comp}, is known, then one can calculate the maximum radius R_{Max} for which the material does not yield the hydrostatic pressure (Beitz et al. 2016)

$$R_{Max} = \sqrt{\frac{3p_{comp}}{2\pi G\rho^2}}, \tag{56}$$

with ρ being the constant mass density in the interior of the body. The compressional strength p_{comp} of dusty material is on the order of 10^7 Pa (Beitz et al. 2013). Thus, hydrostatic or impact pressures exceeding this value are required to remove the microporosity within the dusty material. For a mass density ρ of 2000 Kg m^{-3}, R_{Max} is 133 km. This means that primordial bodies in the AB with radii below 130 km would be undifferentiated asteroids of constant density.

We compute the collision frequency of small asteroids impacting an asteroid of radius 100 km with initial volume filling factor ϕ of 0.6, corresponding to random close packing (Beitz et al. 2016). The number of impacts on a target of radius R per unit time is

$$\frac{dN_p(r_i, r_{i+1})}{dt} = N_v(r_i, r_{i+1})\pi R^2 v_i, \tag{57}$$

where $N_v(r_i, r_{i+1})$ is the number of asteroids per unit volume in a bin of impactor radius $[r_i, r_{i+1}]$ in the main AB extending from 2.2 AU to 3.27 AU (Beitz et al. 2016; Parisi et al. 2016). Since we are taking the averaged number of asteroids per unit volume of the whole AB which only depends on the impactor radii, Eq. (57) will increase with v_i. The square of the impact velocity v_i^2 is computed as $v_i^2 = v_{DS}^2(p, T) + v_e^2$, where $v_e^2 = 2G(m_i + M)/(r_i + R)$ is the square of the mutual escape velocity between the projectile with mass m_i and the target with mass M at the point of contact and $v_{DS}^2(p, T)$ is the square of the relative velocity, i.e., $v_{DS}^2(p, T) = v_{DS}^2(p) + v_{DS}^2(T)$, where $v_{DS}^2(p)$ and $v_{DS}^2(T)$ are the square of the dispersion velocity given by Eq. (26) for the projectile and target eccentricities and inclinations (e_p, i_p) and (e_T, i_T), respectively.
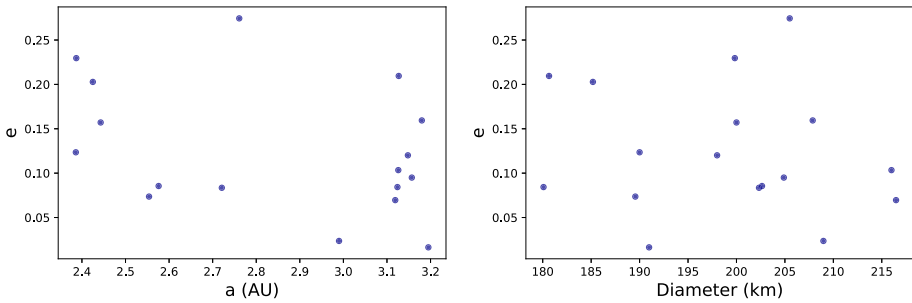
Fig. 7 Eccentricity versus semimajor axis (Left) and eccentricity versus diameter (Right) of Main Belt asteroids with diameters in the range between 180 km and 220 km. Source: https://ssd.jpl.nasa.gov/tools
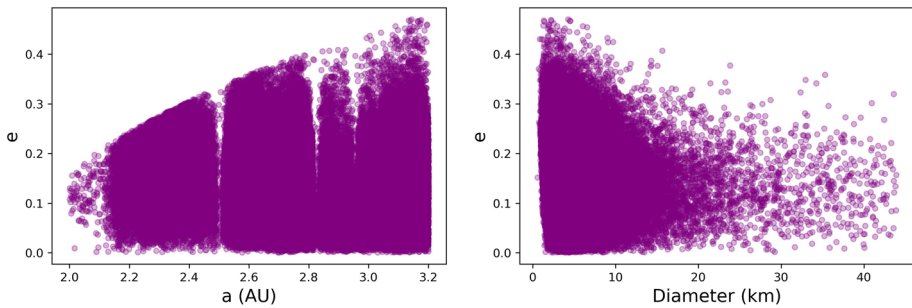

Fig. 8 Eccentricity versus semimajor axis (Left) and eccentricity versus diameter (Right) of Main Belt asteroids with diameters smaller than 44 km. Source: https://ssd.jpl.nasa.gov/tools

We divide the AB into three semimajor axis zones, whose boundaries are given by the ν_6 secular resonance with Saturn, and the 3:1, 5:2 and 2:1 mean motion resonances with Jupiter Morbidelli et al. (2002):
-Inner Ring (IR), between the ν_6 and 3:1 resonances, from 2.2 to 2.5 AU. -Middle Ring (MR), between the 3:1 and 5:2 resonances, from 2.5 to 2.8 AU. -Outer Ring (OR), between the 5:2 and 2:1 resonances, from 2.8 to 3.27 AU.

In computing $v_{DS}^2(p, T)$, we take a_0=(2.2+2.5)/2 AU for the IR, a_0=(2.5+2.8)/2 AU for the MR, and a_0=(2.8+3.27)/2 AU for the OR. Figures 7 and 8 show the distribution in semimajor axis, eccentricity space (left panels of both figures) and the distribution in diameter, eccentricity space (right panels of both figures) of main-belt asteroids with diameters in the range between 180 km and 220 km (target), and with diameters smaller than 44 km (projectiles), respectively.

In order to calculate $v_{DS}^2(p)$, we adopt $(e_p, i_p) = (e_{max}, i_{max})$ from Tables 4, 5 and 6 that are the most frequent values of the eccentricities and inclinations for each range of diameters in the IR, MR and OR, respectively. Analogously, we compute $v_{DS}^2(T)$ assuming $e_T = 0.083$ and $i_T = 0.27$ which are the most frequent values for asteroids of diameters in the range between 180 and 220 km.[2]

The total number of impacts in each impactor bin size over the age of the solar system is computed (Beitz et al. 2016; Parisi et al. 2016)

$$N_{col}(r_i, r_{i+1}) = \frac{dN_p(r_i, r_{i+1})}{dt} 4.5 Gyrs. \tag{58}$$

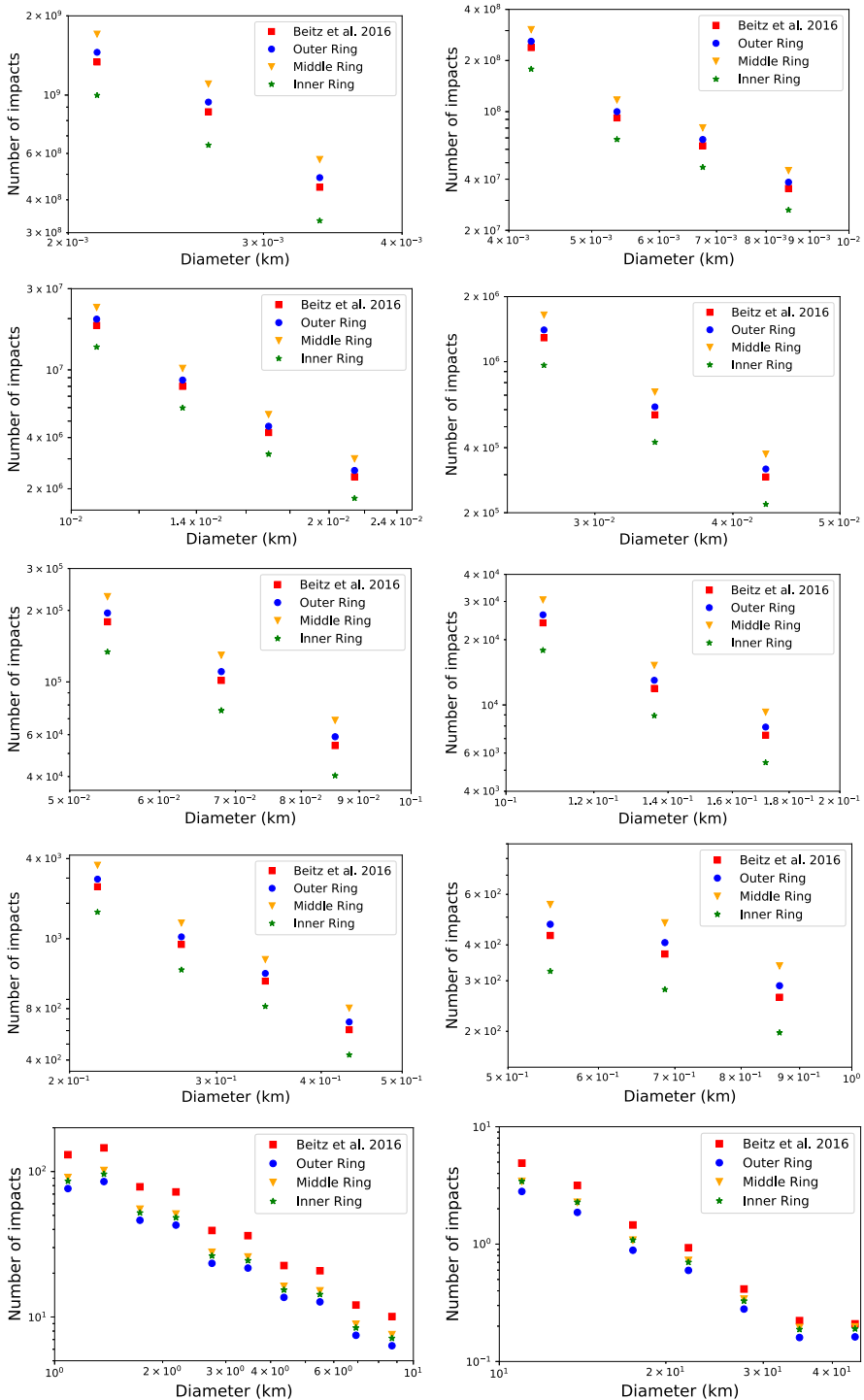_____

[2] https://ssd.jpl.nasa.gov/tools.

Fig. 9 Number of impacts N_{col} of projectiles with radii in the range between 1×10^{-3} km and 22 km on a target of 100 km radius over 4.5 Gyrs for the Inner, Middle and Outer Ring, compared to the results obtained in Beitz et al. (2016)

Table 4 Eccentricities e_{max} and inclinations i_{max} of asteroids in the Inner Ring for different diameter d ranges

	d<1 km	1 km<d<10 km	10 km<d<20 km	20 km<d<44 km
e_{max}	0.284	0.173	0.151	0.093
i_{max}	0.088	0.086	0.07	0.09

Table 5 Eccentricities e_{max} and inclinations i_{max} of asteroids in the Middle Ring for different diameter d ranges

	d<1 km	1 km<d<10 km	10 km<d<20 km	20 km<d<44 km
e_{max}	0.369	0.128	0.15	0.14
i_{max}	0.546	0.21	0.13	0.14

Table 6 Eccentricities e_{max} and inclinations i_{max} of asteroids in the Outer Ring for different diameter d ranges

	d<1 km	1 km<d<10 km	10 km<d<20 km	20 km<d<44 km
e_{max}	0.43	0.076	0.09	0.1
i_{max}	0.43	0.157	0.03	0.04
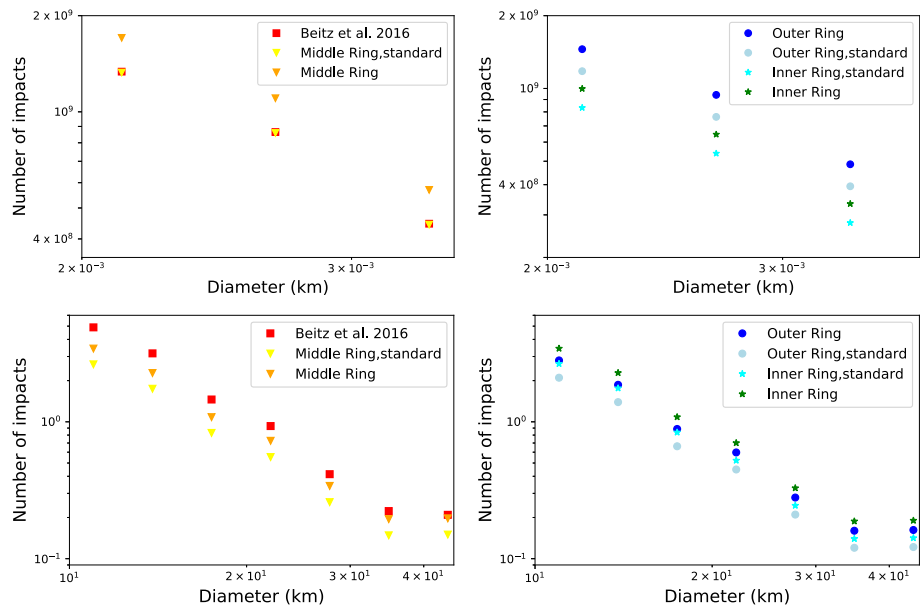
Fig. 10 Number of impacts N_{col} of projectiles with radii in the range between 1×10^{-3} km and 2×10^{-3} km (Upper panel) and between 5 km and 22 km (Bottom panel) on a target of 100 km radius over 4.5 Gyrs for the Inner, Middle and Outer Ring, compared to the results obtained in Beitz et al. (2016) and to the results using the standard dispersion velocity

In Fig. 9, N_{col} is shown for projectiles in the IR, MR and OR, where the results obtained in Beitz et al. (2016) are included. We can see that for projectiles larger than 1 km in diameter the number of impacts computed by Beitz et al. (2016) is higher than the ones here calculated for the IR, MR, and OR. We can also observe that in particular for smaller projectile sizes, there are significant differences between the number of impacts calculated for the IR, MD, and OR. For diameters smaller than 1 km, the separations between the points increase due to the increase in eccentricity.

In Fig. 10, N_{col} is shown for projectiles with radii in the range between 1×10^{-3} km and 2×10^{-3} km and between 5 km and 22 km for the IR, MR and OR, where the results obtained in Beitz et al. (2016) and the results computing v_i with the relative velocity $v_{3std}(p, T)$ are also shown for comparison. The square of the relative velocity $v_{3std}^2(p, T)$ is $(v_{3std}^2(p) + v_{3std}^2(T))$, where $v_{3std}^2(p)$ and $v_{3std}^2(T)$ are given by the standard dispersion velocity (Eq. (33)) for the projectile and target eccentricities and inclinations (e_p, i_p) and (e_T, i_T), respectively. In the left panel of Fig. 10, N_{col} is shown for the MR since in Beitz et al. (2016) the target was placed at the MR, where in the upper panel the results by Beitz et al. (2016) are the same as in the case of the MR by using the standard dispersion velocity, while in the lower panel the number of impacts computed by Beitz et al. (2016) is higher. In the right panel of Fig. 10, the differences in the OR increase with decreasing projectile size for small impactors due to increase in eccentricity.

5.3 Numerical calculation of giant planet formation with planetesimal fragmentation

In a series of previous works (Guilera et al. 2010, 2014), we developed a numerical model that describes the formation of giant planets immersed in a protoplanetary disk that evolves in time. In our model, the protoplanetary disk is represented by a gaseous and a solid component. Planets grow by simultaneous accretion of solids and gas. The solid component of the disk evolves by planet accretion, radial drift due to nebular drag, and collisional evolution, while the gaseous component evolves by an exponential decay. Our planetesimal fragmentation model developed in Guilera et al. (2014) was improved by San Sebastián et al. (2019) incorporating several processes and different velocity regime models for the calculation of low and high relative planetesimal velocities. The number of collisions among planetesimals was computed in San Sebastián et al. (2019) by Eq. (42) in the high-velocity regime (see Section 2.2.1 and Appendix B.1 in San Sebastián et al. (2019)), and the protoplanet accretion rate was computed following (Inaba et al. 2001) (see Appendix A.2 in San Sebastián et al. (2019)), where the square relative velocity between a planetesimal and the embryo was computed as v_{3std}^2 (Eq.(33)). Since we have shown (San Sebastián et al. 2019) that the high-velocity regime is dominant, our model is here improved with the inclusion of our calculation of the dispersion velocity v_{DS} developed in Sect. 3.2.

Our simulations start with a disk ten times more massive than the minimum solar nebula at the beginning of the oligarchic growth with a moon-sized embryo located at 5 AU from the central star that is immersed in an homogeneous single-sized population of nonporous planetesimals of 100 km radius. The simulations stop when the crossover mass is achieved. We present in this paper the results of the simulation including v_{DS}^2 expanded around $e = 0$ up to sixth order in e ($V_{DS(6th)}^2$) for the high-velocity regime, where the baseline case for this work is the same as in San Sebastián et al. (2019).

The evolution of the protoplanet mass is shown in Fig. 11, where we can observe that the protoplanet achieves the crossover mass at a longer time than in the baseline case (top panel),

Fig. 11 Core masses (solid lines) and envelope masses (dashed lines) as a function of time. Gray lines: model with no planetesimal fragmentation. Red lines: baseline model. Pink lines: baseline model with $V_{DS(6th)}^2$. Black lines: model with no planetesimal fragmentation and $V_{DS(6th)}^2$. Top panel: Time evolution of the protoplanet mass until it achieves the crossover mass. Bottom panel: same as top panel but until 2 Myr
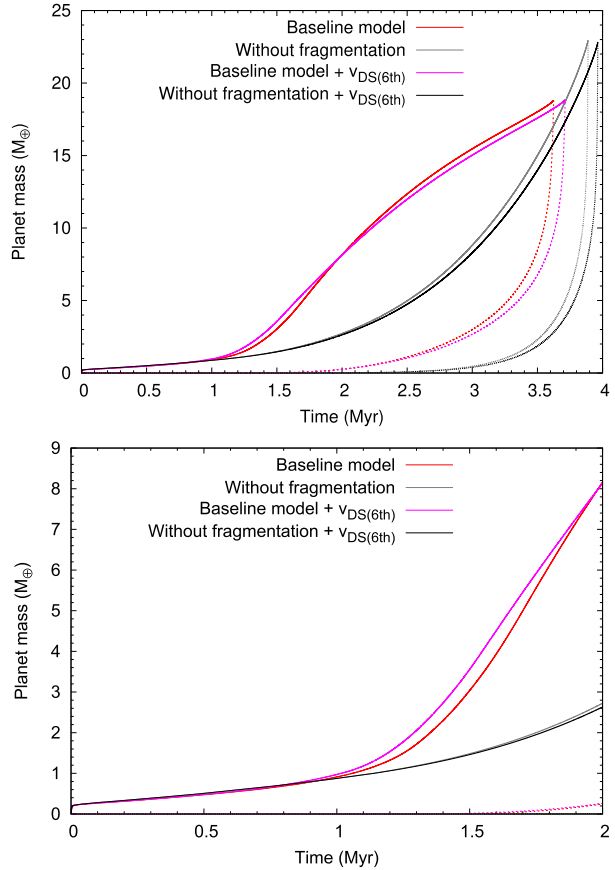
although the protoplanet growth increases slightly with respect to the baseline case within the first millions years (bottom panel).

In Fig. 12 (left), the relative velocity of 100-km-radius planetesimals is shown. The increased collision velocity (with respect to the baseline case) generates that 100-km-radius planetesimals reach the necessary energy to fragment due to collisions at an earlier time, which follows from Fig. 12 (right). The figure shows the time evolution of the mean value of the surface density of 100-km-radius planetesimals for the baseline case and for the simulation where $V_{DS(6th)}^2$ is included. We can see that the surface density for the case with $V_{DS(6th)}^2$ decreases at an earlier time than in the baseline case since the initial 100 km-sized planetesimals start to fragment earlier due to the increased collision velocity.

The time evolution of the relative velocity among planetesimals for the baseline model and for $V_{DS(6th)}$ is shown in Fig. 13 for planetesimals of 1 km and 1 m radii. We can see that the relative velocity among planetesimals decreases with decreasing planetesimal radius due to damping by gas drag in the baseline case (Chambers 2006; San Sebastián et al. 2019) as well as in the case where $V_{DS(6th)}$ is included. In Figs. 14 and 15, we show the time evolution of the mean surface density and the accretion rates for km-radius and m-radius planetesimals. We can see that the surface density for the case in which $V_{DS(6th)}^2$ is included increases during the first 1.5 Myrs with respect to the baseline case since planetesimals fragment earlier due
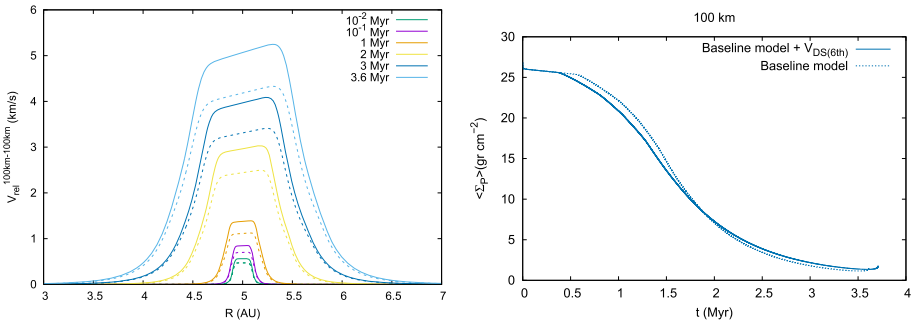
Fig. 12 Left: Time evolution of the relative velocity among 100-km-radius planetesimals for the baseline model (dashed lines) and for $V_{DS(6th)}$ (solid lines). Right: Time evolution of the mean value of the surface density of 100-km-radius planetesimals for the baseline model (dashed line) and the case where $V_{DS(6th)}^{2}$ is included (solid line)
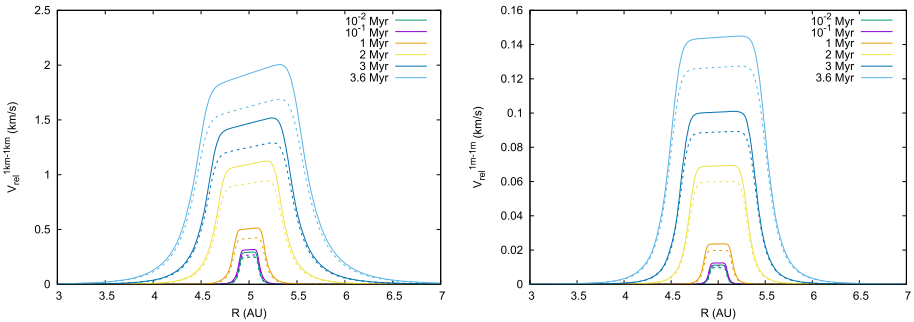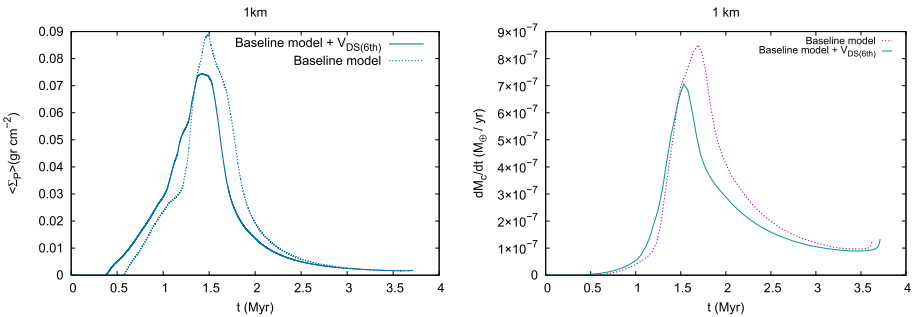

Fig. 13 Time evolution of the relative velocity among planetesimals for the baseline model (dashed lines) and for $V_{DS(6th)}$ (solid lines). Left: 1 km-radius planetesimals. Right: 1 m-radius planetesimals

Fig. 14 Left: Time evolution of the mean value of the surface density of 1-km-radius planetesimals for the baseline case (dashed line) and the case where $V_{DS(6th)}$ is included (solid line). Right: Accretion rate as function of time of 1-km-radius planetesimals for the baseline case (dashed line) and the case where $V_{DS(6th)}$ is included (solid line)
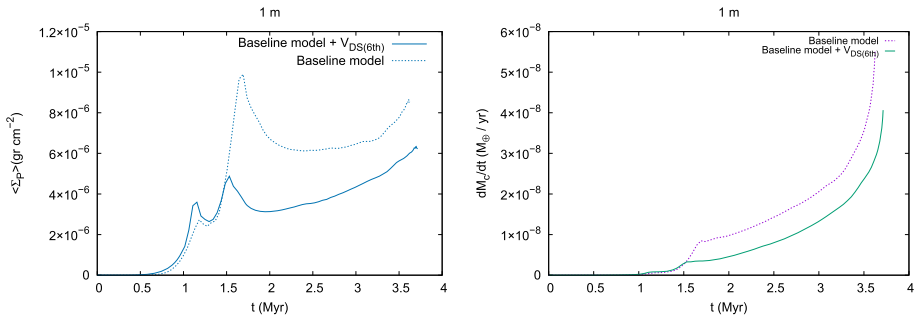
Fig. 15 Left: Time evolution of the mean value of the surface density of 1-m-radius planetesimals for the baseline case (dashed line) and the case where $V_{DS(6th)}$ is included (solid line). Right: Accretion rate as function of time of 1-m-radius planetesimals for the baseline case (dashed line) and the case where $V_{DS(6th)}$ is included (solid line)

to increased collision velocity, increasing the number of smaller planetesimals. We can also observed that the accretion rates are slightly higher for the case in which $V^2_{DS(6th)}$ is included during the first 1.5 Myrs. During the later evolution, surface densities and accretion rates decrease for the case with $V^2_{DS(6th)}$ (with respect to the baseline case) not only due to the fragmentation process but also because planetesimals are subject to an increased perturbation (increased relative velocity), and then, some of them will not participate in the formation of the embryo being scattered out of the embryo feeding zone.

6 Conclusions

The dispersion velocity plays a key role in analytical as well as in numerical models of the collisional evolution of planetesimals, ABs and KBs, as well as in the calculation of protoplanets accretion rates.

We calculate a general and complete analytical expression of the square of the dispersion velocity, which may be expanded as a power series around any value of the orbital eccentricity e and which is an exact solution for any value of the orbital inclination i, that may be useful to study several aspects of the planetary and satellite formation and evolution processes.

We expanded our expression of the square of the dispersion velocity around $e = 0$ up to sixth order in e to analyze in a simple semianalytical way the behavior of accretion rates and collision probabilities in a gas free environment. We find that our results of solid accretion rates and collision probabilities are lower than previous estimates where the particle-in-a-box approach has been applied. Our models of the formation of a giant planet with planetesimal fragmentation in a gaseous disk (San Sebastián et al. 2019) and of the collision frequency on undifferentiated large asteroids (Beitz et al. 2016; Parisi et al. 2016) are here improved by using our expression of the square of the dispersion velocity up to sixth order in e. We find, on the one hand, that the protoplanet achieves the crossover mass at a longer time than previous cases where the standard dispersion velocity usually adopted in the literature has been used. Such result confirms the predictions found from our semianalytical approach. On the other hand, our model of the collision frequency on undifferentiated large asteroids is here improved by using in our calculation of the dispersion velocity the updated distribution of eccentricities and inclinations as function of the impactor and target radii in the inner, middle and outer asteroid belt.

The analytical equations presented in this paper offer a rigorous calculation of relative velocities among minor bodies, which, in principle, might provide more accurate results for planned space missions.

A Jacobi integral

A.0.1 Planar case

In the frame of the restricted three-body problem (Danby 1992; Kaula 1968) for orbital inclination $i = 0^o$, the square of the relative velocity v_{2Saf}^2 in the protoplanet rotational system is given by Safronov (1972):

$$v_{2Saf}^2 = v_0^2 \left[3 - \left(\frac{1 - e^2}{1 + e \cos \varphi} \right) - 2(1 + e \cos \varphi)^{1/2} \right]. \tag{59}$$

We average Eq. (59) over one orbital period as:

$$< v_{2Saf}^2 > = \frac{1}{2\pi} \int_0^{2\pi} (v_{2Saf}^2) \, d\varphi. \tag{60}$$

Then,

$$\langle v_{2Saf}^2 \rangle = v_0^2 \left[3 - \left\langle \frac{1 - e^2}{1 + e \cos \varphi} \right\rangle - 2 \left\langle (1 + e \cos \varphi)^{1/2} \right\rangle \right], \tag{61}$$

where

$$\left\langle \frac{1 - e^2}{1 + e \cos \varphi} \right\rangle = (1 - e^2)^{1/2}. \tag{62}$$

Substituting Eqs. (62) and (17) in Eq. (61), we arrive to Eq.(18), i.e., $\langle v_{2Saf}^2 \rangle = v_{DP}^2$.

A.0.2 Spatial case

In a reference system rotating with the protoplanet around the star, the squared relative velocity v_{3Saf}^2 of a planetesimal with an eccentric, inclined orbit with respect to the circular orbit of the protoplanet (Danby 1992; Kaula 1968) at the point of intersection of the orbits is given by

$$v_{3Saf}^2 = v_0^2 \left[3 - \left(\frac{1 - e^2}{1 + e \cos \varphi} \right) - 2 \cos i (1 + e \cos \varphi)^{1/2} \right]. \tag{63}$$

If $i = 0^o$, Eq. (63) equals Eq. (59), i.e., $v_{D3Saf}^2 = v_{D2Saf}^2$. Averaging Eq. (63) over one orbital period

$$\langle v_{3Saf}^2 \rangle = v_0^2 \left[3 - \left\langle \frac{1 - e^2}{1 + e \cos \varphi} \right\rangle - 2 \cos i \left\langle (1 + e \cos \varphi)^{1/2} \right\rangle \right], \tag{64}$$

and substituting Eq. (62) in the second term and Eq. (17) in the third term of the right hand of Eq. (64), we arrive to Eq. (25), i.e., $\langle v_{3Saf}^2 \rangle = v_{DS}^2$. Note that when $i = 0^o$, $v_{DS}^2 = v_{DP}^2 = \langle v_{2Saf}^2 \rangle = \langle v_{3Saf}^2 \rangle$.

B Planar case plus the average over a vertical oscillation

The epicyclic approximation (Binney and Tremaine 1987) describes the motion of a particle in the meridional plane, where the particle motion is given by a simple harmonic oscillation in the XY plane plus a simple harmonic oscillation in the vertical direction. In a similar way, for $(e, i) << 1$, the square of the standard dispersion velocity in space v_{3sdt}^2 (the square of Eq. (33), Lissauer and Stewart (1993)) may be obtained as the first term of Eq. (19) plus the contribution of the average over a vertical oscillation.

From Fig. 1, the vertical component of the planetesimal position measured with respect to the XY plane is

$$z = R \sin(\omega + \varphi) \sin i. \tag{65}$$

Then, deriving Eq. (65)

$$\dot{z} = \dot{R} \sin(\omega + \varphi) \sin i + R\dot{\varphi} \cos(\omega + \varphi) \sin i. \tag{66}$$

Substituting Eqs. (7) and (8), in Eq. (66) we obtain

$$\dot{z} = \frac{v_0 \sin i}{(1 - e^2)^{1/2}(1 + \tilde{a})^{1/2}}[(1 + e \cos \varphi) \cos(\omega + \varphi)$$
$$+ e \sin \varphi \sin(\omega + \varphi)]. \tag{67}$$

Substituting Eq. (9) in Eq. (67), rising to the square and averaging in the way shown in Eq. (13), we get

$$\langle \dot{z}^2 \rangle = v_0^2 \sin^2 i \left(1 - \frac{(1 - e^2)^{1/2}}{2}\right). \tag{68}$$

Finally, developing Eq. (68) in power series around $(e = 0, i = 0)$, approximating $\sin i \sim i$, adding the first term of Eq. (19) and keeping terms up to second order in (e,i), we arrive to the square of Eq. (33).

References

Adachi, I., Hayashi, C., Nakazawa, K.: The gas drag effect on the elliptical motion of a solid body in the primordial solar nebula. Progress Theoret. Phys. **56**, 1756–1771 (1976). https://doi.org/10.1143/PTP.56.1756

Beitz, E., Blum, J., Parisi, M.G., Trigo-Rodriguez, J.: The collisional evolution of undifferentiated asteroids and the formation of chondritic meteoroids. Ap. J. **824**(1), 12 (2016). https://doi.org/10.3847/0004-637X/824/1/12

Beitz, E., Güttler, C., Nakamura, A.M., Tsuchiyama, A., Blum, J.: Experiments on the consolidation of chondrites and the formation of dense rims around chondrules. Icarus **225**(1), 558–569 (2013). https://doi.org/10.1016/j.icarus.2013.04.028

Binney, J., Tremaine, S.: Galactic dynamics (1987)

Bottke, W.F., Durda, D.D., Nesvorný, D., Jedicke, R., Morbidelli, A., Vokrouhlický, D., Levison, H.: The fossilized size distribution of the main asteroid belt. Icarus **175**, 111–140 (2005). https://doi.org/10.1016/j.icarus.2004.10.026

Chamberlin, A.B.: JPL's Asteroid and Comet Database - Custom Web-based Tools. In: AAS/Division for Planetary Sciences Meeting Abstracts #40, *Bulletin of the American Astronomical Society*, vol. 40, p. 435 (2008)

Chambers, J.: A semi-analytic model for oligarchic growth. Icarus **180**(2), 496–513 (2006). https://doi.org/10.1016/j.icarus.2005.10.017

Chambers, J.E.: Giant planet formation with pebble accretion. Icarus **233**, 83–100 (2014). https://doi.org/10.1016/j.icarus.2014.01.036

Czechowski, Z., Leliwa-Kopystyński, J., Teisseyre, R.: Rise of planetary bodies. In: R. Teisseyre, J. Leliwa-Kopystyński, B. Lang (eds.) Evolution of the Earth and Other Planetary Bodies: Physics and Evolution of the Earth's Interior 5, pp. 51–187 (1992)

Danby, J.M.A.: Fundamentals of celestial mechanics (1992)

Gomes, R., Levison, H.F., Tsiganis, K., Morbidelli, A.: Origin of the cataclysmic Late Heavy Bombardment period of the terrestrial planets. Nature **435**(7041), 466–469 (2005). https://doi.org/10.1038/nature03676

Greenberg, R., Bottke, W.F., Carusi, A., Valsecchi, G.B.: Planetary accretion rates—analytical derivation. Icarus **94**, 98–111 (1991). https://doi.org/10.1016/0019-1035(91)90143-H

Greenzweig, Y., Lissauer, J.J.: Accretion rates of protoplanets. Icarus **87**, 40–77 (1990). https://doi.org/10.1016/0019-1035(90)90021-Z

Grishin, E., Perets, H.B.: Application of gas dynamical friction for planetesimals. I. Evolution of single planetesimals. Apj **811**(1), 54 (2015). https://doi.org/10.1088/0004-637X/811/1/54

Guilera, O.M., Brunini, A., Benvenuto, O.G.: Consequences of the simultaneous formation of giant planets by the core accretion mechanism. Astron. Astrophys. **521**, A50 (2010). https://doi.org/10.1051/0004-6361/201014365

Guilera, O.M., de Elía, G.C., Brunini, A., Santamaría, P.J.: Planetesimal fragmentation and giant planet formation. Astron. Astrophys. **565**, A96 (2014). https://doi.org/10.1051/0004-6361/201322061

Guilera, O.M., Fortier, A., Brunini, A., Benvenuto, O.G.: Simultaneous formation of solar system giant planets. Astron. Astrophys. **532**, A142 (2011). https://doi.org/10.1051/0004-6361/201015731

Ida, S., Guillot, T., Morbidelli, A.: Accretion and destruction of planetesimals in turbulent disks. Astrophys. J. **686**, 1292–1301 (2008). https://doi.org/10.1086/591903

Ida, S., Makino, J.: Scattering of planetesimals by a protoplanet: slowing down of runaway growth. Icarus **106**(1), 210–227 (1993). https://doi.org/10.1006/icar.1993.1167

Inaba, S., Tanaka, H., Nakazawa, K., Wetherill, G.W., Kokubo, E.: High-accuracy statistical simulation of planetary accretion: II. Comparison with N-body simulation. Icarus **149**, 235–250 (2001). https://doi.org/10.1006/icar.2000.6533

Jutzi, M., Michel, P., Benz, W., Richardson, D.C.: Fragment properties at the catastrophic disruption threshold: the effect of the parent body's internal structure. Icarus **207**(1), 54–65 (2010). https://doi.org/10.1016/j.icarus.2009.11.016

Kaula, W.M.: An introduction to planetary physics - The terrestrial planets (1968)

Levison, H.F., Bottke, W.F., Gounelle, M., Morbidelli, A., Nesvorný, D., Tsiganis, K.: Contamination of the asteroid belt by primordial trans-Neptunian objects. Nature **460**(7253), 364–366 (2009). https://doi.org/10.1038/nature08094

Lissauer, J.J., Stewart, G.R.: Growth of planets from planetesimals. In: E.H. Levy, J.I. Lunine (eds.) Protostars and Planets III, pp. 1061–1088 (1993)

Morbidelli, A., Bottke W. F., J., Froeschlé, C., Michel, P.: Origin and Evolution of Near-Earth Objects. In: Asteroids III, pp. 409–422 (2002)

Morbidelli, A., Bottke, W.F., Nesvorný, D., Levison, H.F.: Asteroids were born big. Icarus **204**, 558–573 (2009). https://doi.org/10.1016/j.icarus.2009.07.011

Murray, C.D., Dermott, S.F.: Solar system dynamics (1999)

Parisi, M.G.: Impact disruption of primordial planetesimals. Planet. Space Sci. **75**, 96–104 (2013). https://doi.org/10.1016/j.pss.2012.09.013

Parisi, M.G., Beitz, E., Blum, J.: Compaction, cratering and collision frequency on chondritic parent objects. Boletin de la Asociacion Argentina de Astronomia La Plata Argentina **58**, 313–315 (2016)

Ronco, M.P., de Elía, G.C.: Formation of Solar system analogues - II. Post-gas-phase growth and water accretion in extended discs via N-body simulations. MNRAS **479**(4), 5362–5384 (2018). https://doi.org/10.1093/mnras/sty1773

Safronov, V.S.: Evolution of the protoplanetary cloud and formation of the earth and planets. (1972)

San Sebastián, I.L., Guilera, O.M., Parisi, M.G.: Planetesimal fragmentation and giant planet formation. II. Dependencies with planetesimal relative velocities and compositions. Astron. Astrophys. **625**, A138 (2019). https://doi.org/10.1051/0004-6361/201834168

Stern, S.A.: On the collisional environment, accretion time scales, and architecture of the massive, primordial Kuiper belt. AJ **112**, 1203 (1996). https://doi.org/10.1086/118091

Stern, S.A.: Signatures of collisions in the Kuiper disk. Astron. Astrophys. **310**, 999–1010 (1996)

Stern, S.A., Colwell, J.E.: Accretion in the Edgeworth-Kuiper belt: forming 100–1000 KM radius bodies at 30 AU and beyond. Astron. J. **114**, 841 (1997). https://doi.org/10.1086/118518

Tsiganis, K., Gomes, R., Morbidelli, A., Levison, H.F.: Origin of the orbital architecture of the giant planets of the Solar System. Nature **435**(7041), 459–461 (2005). https://doi.org/10.1038/nature03539

Weidenschilling, S.J.: Initial sizes of planetesimals and accretion of the asteroids. Icarus **214**, 671–684 (2011). https://doi.org/10.1016/j.icarus.2011.05.024

Wetherill, G.W., Stewart, G.R.: Formation of planetary embryos—effects of fragmentation, low relative velocity, and independent variation of eccentricity and inclination. Icarus **106**, 190 (1993). https://doi.org/10.1006/icar.1993.1166